Geomechanics and Engineering, *Vol. 36, No. 4 (2024) 343-353*
https://doi.org/10.12989/gae.2024.36.4.343

Factors affecting hydraulic anisotropy of soil

Nurly Gofar[1a], Alfrendo Satyanaga[*2], Gerarldo D. Aventian[2b], Gulnur Pernebekova[2c], Zhanat Argimbayeva[2d], Sung-Woo Moon[2e] and Jong Kim[2f]

[1]*Department of Civil Engineering, Post Graduate Program, Universitas Bina Darma, Palembang 30111, Indonesia*
[2]*Department of Civil and Environmental Engineering, Nazarbayev University, Astana 010000, Kazakhstan*

(*Received August 9, 2022, Revised November 21, 2023, Accepted December 30, 2023*)

Abstract. The hydraulic anisotropic behavior of unsaturated soil has not been fully explored in relation to the grain-size distribution. The present study conducted laboratory assessments to examine the hydraulic anisotropy condition of statically compacted specimens in various initial states. The investigation incorporated the concept of hydraulic anisotropy by employing two discrete forms of soil stratification: horizontal-layering (HL) and vertical-layering (VL). The examined soils comprised sandy silt and silty sand, exhibiting either unimodal or bimodal soil-water characteristic curve (SWCC). This study aimed to investigate the potential correlation between the hydraulic anisotropy ratio and soil properties. The present study established a correlation between the hydraulic anisotropy ratio and several soil parameters, including fine content, dry density, plastic limit, and liquid limit. The study results indicate a non-linear relationship between the percentage of fine and dry density in soils with unimodal and bimodal soil-water characteristic curve (SWCC) and hydraulic anisotropy ratio.

Keywords: #hydraulic anisotropy; permeability; soil properties; soil-water characteristic curve; unimodal and bimodal soil; unsaturated soil

1. Introduction

The soil-water characteristic curve (SWCC) is an essential soil parameter that can be analyzed to determine the behavior of the soil (Deng *et al.* 2019). It is the graphical representation of the relationship between the soil's water content and water potential, also known as soil suction (Al-Mahbashi *et al.* 2015). The shape of SWCC is affected by the initial void ratio and dry density of the soil (Zhai *et al.* 2023, Zhai *et al.* 2020a). Therefore, currently there are two distinct configurations of SWCC: the unimodal configuration, characterized by a solitary curve (namely, the sigmoid), and the bimodal configuration, which encompasses two subsidiary curves. The generation of a unimodal form of SWCC can be observed in gap-graded soil that has been compacted at a dry density associated with the wet of optimal, as indicated by the findings of Satyanaga *et al.* (2022), Priono *et al.* (2016a), and Zhai *et al.* (2020b) in their respective studies. Conversely, when gap-graded soil is compacted at the dry of optimum, it will result in a bimodal configuration of SWCC (Krisnanto *et al.* 2020, Hamdany *et al.* 2023). In other words, soil exhibiting a unimodal soil water characteristic curve (SWCC) is characterized by a flocculated particle arrangement, whereas soil displaying a bimodal SWCC indicates a dispersed organization. The hydraulic anisotropy of soil may exhibit dissimilar behavior between unimodal and bimodal soil water characteristic curves due to variations in particle arrangement. SWCC can be associated with the drying and wetting process (Zhai *et al.* 2020c). However, Satyanaga and Rahardjo (2022) indicated that drying SWCC provided a higher contribution to factor of safety of slope as compared to wetting SWCC. Therefore, this study focuses on drying SWCC.

Soil anisotropy is a phenomenon that has been studied by several researchers (Basak 1972, Mualem 1986, Chapuis *et al.* 1989, Bear and Cheng 2010, Priono *et al.* 2016a). It is characterized by the variation in water permeability coefficients along the major and minor axes of the soil. The primary axis denotes the orientation that runs parallel to the soil strata, whereas the secondary axis denotes the orientation that runs perpendicular to the soil strata (Qi *et al.* 2019). The hydraulic anisotropy of soil may exhibit either isotropic characteristics, where the value is equivalent to one, or anisotropic characteristics, where the value is greater or lesser than one. In most cases, the hydraulic anisotropy of soil is observed to be greater than one, except for clays located at shallow depths that contain numerous roots and wormholes, as noted by Bear and Cheng (2010). Laboratory studies on pure saturated rock, sand, and clay

∗Corresponding author, Assistant Professor
E-mail: alfrendo.satyanaga@nu.edu.kz
[a]Professor
E-mail: nurly_gofar@binadarama.ac.id
[b]Research Scholar
E-mail: gerarldo.aventian@nu.edu.kz
[c]Research Scholar
E-mail: gulnur.pernebekova@nu.edu.kz
[d]Research Scholar
E-mail: zhanat.argimbayeva@nu.edu.kz
[e]Assistant Professor
E-mail: sung.moon@nu.edu.kz
[f]Professor
E-mail: jong.kim@nu.edu.kz

ISSN: 2005-307X (Print), 2092-6219 (Online)

conducted by Basak (1972) and Chapuis *et al.* (1989) have indicated a maximum value of four for inherent hydraulic anisotropy. The proposal put forth by Basak (1972) suggests that hydraulic anisotropy ratios in clay may vary depending on whether the soil structure is flocculated or scattered.

Prior studies, including those conducted by Mualem (1984), Ursino *et al*. (2000), and Assouline and Or (2006), sought to understand the behavior of hydraulic anisotropy in unsaturated conditions. These studies proposed conceptual models and conducted analytical or numerical analyses across various scenarios. The concept of a soil model consisting of multiple thin parallel layers, each possessing unique hydraulic properties, was introduced by Mualem (1984) and is commonly referred to as the "layered cake" model. The saturated permeability function of multiple layers was represented using a uniform density distribution function (Rahardjo *et al.* 2009). The hydraulic anisotropic behavior was observed by postulating a power function correlation between the permeability and the matric suction.

The study conducted by Ursino *et al.* (2000) investigated three potential arrangements of anisotropy in porous media that are similar to Miller's. The study revealed that solely the distribution of pore diameter might exhibit anisotropy, exclusively the density of pores may display anisotropy, or both the density and the pore-size distribution (PSD) may manifest anisotropy. Roth and Hammel (1996) described a situation subjected to numerical simulations, wherein the hydraulic anisotropy resulting from different configurations was considered. Mualem (1984) and Ursino *et al.* (2000) have observed that the hydraulic anisotropic behavior can be dependent or independent of saturation conditions determined by the present configurations. Assoluine and Or (2006) modified the layered cake model to incorporate the impact of variations in bulk density within a specific soil category. This action was undertaken to investigate the ramifications of climate change.

However, previous research has not thoroughly investigated the hydraulic anisotropy of soil with different grain size distributions, which has predominantly focused on a single soil combination. It is anticipated that the results of this study will broaden our understanding of the connection between the hydraulic anisotropy properties of soil and the fine content of that soil. The purpose of this investigation is to study the relationship between hydraulic anisotropy ratio and soil attributes based on the shape of SWCC and the permeability of the soil. Examining the hydraulic anisotropy ratio of sand-kaolin mixes with varied compositions related to unimodal and bimodal SWCC is the only thing that falls under the purview of this project's scope. To investigate the connection between hydraulic anisotropy and soil parameters for a variety of different soil combinations, statistical studies were carried out.

2. Applicable theory

There is a substantial relationship between permeability and hydraulic anisotropy (Kim and Jeong 2017). Hydraulic anisotropy, on the other hand, represents the permeability ratio parallel and perpendicular to soil layers. This ratio is expressed by the expression of $k_{parallel/kperpendicular}$ (Bear and Cheng 2010), and a high ratio value indicates a larger flow rate in the parallel direction. According to numerous research, soil particle arrangement, or structure, is linked to the hydraulic anisotropy ratio (e.g., Fredlund and Rahardjo 1993). Soil density in a saturated state is one factor that affects the hydraulic anisotropy ratio, as discovered by Basak (1972). Bridging and Ordering can also explain soil structure organization, a phenomenon described by Lee *et al*. (2007). This configuration will immediately affect the value of the hydraulic anisotropy ratio due to the uneven distribution of hydraulic conductivity caused by the platy particles (Deng *et al.* 2020).

It is a justifiable expectation that soils possessing similar compositions, regardless of the orientation of their layering, will produce a corresponding drying soil water characteristic curve (SWCC) that can be optimally accommodated by employing the identical line. Consequently, there is no justification to postulate that the SWCC would be affected by the orientation component.

The equations that provide the most accurate fit for unimodal and bimodal SWCCs in this research are those initially proposed by Fredlund and Xing (1994) and Satyanaga *et al*. (2019a), as presented in Eqs. (1) and (2). The equations were employed to determine the optimal values that best fit the SWCCs. The third parameter (m) in Eq. (1) confers supplementary adaptability by allowing the low matric suction range to possess an autonomous configuration from the high matric suction range, resulting in three fitting parameters. Stated differently, it can be observed that Eq. (1) possesses a total of three parameters that are subject to fitting. Satyanaga *et al*. (2019a) proposed Eq. (2) to address the lack of available equations in the literature for best-fitting bimodal SWCC. Leong and Rahardjo (1997) findings indicate that Eq. (1) can accurately represent experimental data across a broad spectrum of suction values. The study recommended that the correction factor C (ψ) should be set to 1 for practical purposes.

$$\theta_w = C(\psi)\frac{\theta_s}{\left\{ln ln\left[e+\left(\frac{\psi}{a}\right)^n\right]\right\}^m} \tag{1}$$

where a, n, m are fitting parameters; C(ψ) is a correction factor; ψ is soil suction (kPa); θ_s is saturated volumetric water content, and θ_w is a volumetric water content.

$$\theta_w = \left(1-\frac{ln\ ln\left(1+\frac{\psi}{\psi_r}\right)}{ln\ ln\left(1+\frac{10^6}{\psi_r}\right)}\right)[\theta_r + (\theta_{s1}-\theta_{s2})\left(1-erfc\frac{ln\ ln\left(\frac{\psi_{a1}-\psi}{\psi_{a1}-\psi_{m1}}\right)}{s_1}\right) + (\theta_{s2}-\theta_r)\left(1-erfc\frac{ln\ ln\left(\frac{\psi_{a2}-\psi}{\psi_{a2}-\psi_{m2}}\right)}{s_2}\right)] \tag{2}$$

where s is a parameter related to SWCC's geometric standard deviation; ψ_m is a parameter associated with the

matric suction at the point of inflection of SWCC (kPa); erfc is a complementary error function; ψ_a is a parameter related to the air-entry value (AEV) of soil (kPa); The numbers 1 and 2 in the subscripts refer to the first and second sub-curves, respectively, of the bimodal SWCC.

To determine the time needed for equalization during a SWCC test, it is important to construct a systematic criterion in addition to the basic formula. Although the graphical inspection is typically utilized at the end of each matric suction equalization to determine whether the specimen has reached the equilibrium condition, this method has the potential to be extremely subjective. The central difference approximation of the Taylor Series was utilized to support the generally accepted graphical observation (as shown in Eq. (3)). It was determined that the beginning of the equalization process coincided with the first instance in which the gradient of the water volume change curve became zero. This was taken to be the point at which the equalization process got underway.

$$f'(x_i) = O(h^2) + \frac{[f(x_{i+1}) - f(x_{i-1})]}{2h} \quad (3)$$

where $O(h^2)$ is a truncation error; xi is related to time step; h is associated to step size (50 intervals); f (xi) is a gradient of the curve.

3. Materials

Soil mixtures were selected to produce uniform samples to guarantee their uniformity, reliability, and reproducibility (Sharipov *et al.* 2023). Furthermore, it is imperative that the soil composition remains stable and resistant to compression under the influence of significant pressure, as the specimens will be subjected to such conditions. The study utilized ASTM 20-30 grade Ottawa sand and L2 grade coarse kaolin as the primary materials. The sand was chosen as the material because of the granular shape of its particles, which helps save the amount of time required for a number of laboratory experiments, most notably the permeability test. However, kaolin was chosen because of its ability to bind the other ingredients together. Furthermore, kaolin comprises fine-grained particles that can obtain various hydraulic properties in a wide range of matric suctions. Fig. 1 illustrates the photo of the investigated soils.

Several experiments were conducted to evaluate the index properties of the soil for the purpose of classifying the soil mixture using the Unified Soil Classification System (USCS). The experimental procedures encompassed dry sieving and hydrometer analysis with specific gravity tests, Atterberg limits tests, and grain-size distribution tests. All tests were conducted following the guidelines set forth by the ASTM standards. ASTM D854-14 for specific gravity test, ASTM D4318-10 for Atterberg Limit test, ASTM D422-63 for particle size distribution test and ASTM D2487-11 for Unified Soil Classification System (USCS).

In performing a SWCC test, it is imperative to establish a systematic criterion to determine the duration of the equalization phase, in addition to utilizing the fundamental equations. Kaolin can be used for a variety of purposes.

Fig. 1 Kaolin and sand used in the study

This investigation employed three different soil mixtures, 30% sand - 70% kaolin by its dry mass (30S70K), 50% sand - 50% kaolin by its dry mass (50S50K), 70% sand - 30% kaolin by its dry mass (70S30K). It is anticipated that the variation in the soil composition utilized will provide greater insight into the hydraulic anisotropic characteristics of soil with a larger proportion of particles. Another reason to employ this primarily kaolin combination is to prepare for the necessary steps in conducting permeability tests. It is because a low kaolin composition may result in a high permeability soil. According to ASTM D7664-10, the saturated hydraulic conductivity (K_{sat}) of the soil specimen should be less than the K_{sat} of the ceramic disks used in the apparatus to minimize the flow impedance effect.

4. Sample preparation

Prior to specimen preparation, the standard proctor compaction test according to ASTM D698-12e1 was performed to ascertain the compaction curve and establish the initial conditions for preparing the specimen. The tray contained a substantial amount of the soil blend that had been formulated. The partitioning of the test into its various segments was contingent upon the quantity of water present. At each successive stage, a progressively greater quantity of distilled water was incorporated in accordance with the specified percentage. Subsequently, the soil amalgam was compressed into three strata at every moisture level, and the corresponding overall and desiccated densities were ascertained. Water content was quantified by obtaining a specimen from each stratum subsequent to its pulverization. A compaction curve was constructed for the soil amalgamation after gathering all the pre-established data points. The initial state for the preparation of the specimen was selected as 95% of the maximum dry density. Table 1 presents the details of specimens taken from the compaction curve. This action aimed to ensure that the density level of the dry and wet optimum sides on the compaction curve would be equivalent. The optimal distribution's dry and wet sides are expected to produce bimodal and unimodal soil water characteristic curves (SWCC), respectively. The utilization of the figure of 95% was aimed at ensuring comparability with the findings of previous studies conducted by Priono *et al*. (2016a), and Priono *et al.* (2016b), Satyanaga *et al*. (2019b).

On both the dry and wet sides of the optimal point on the compaction curve, the starting conditions for the

Table 1 Soil mixture for dynamic compaction

Specimen #	Specimen Description			Starting Conditions	
	% Sand	% Kaolin	Naming	Wet of optimum	Dry of optimum
1	30	70	30S70K	95% $\gamma_{d, max}$	
2	30	70	30S70K		95% $\gamma_{d, max}$
3	50	50	50S50K	95% $\gamma_{d, max}$	
4	50	50	50S50K		95% $\gamma_{d, max}$
5	70	30	70S30K	95% $\gamma_{d, max}$	
6	70	30	70S30K		95% $\gamma_{d, max}$

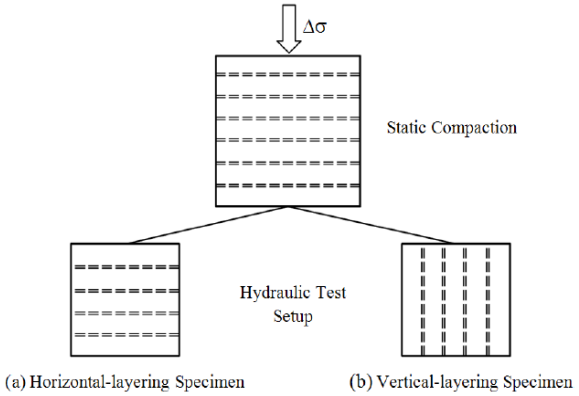

Fig. 2 Schematic diagram of layering within the soil specimens

specimens are set to 95% of the maximum dry density. Quantifying the hydraulic anisotropy of each initial condition will require the production of two distinct types of specimens: those with horizontal layering (HL) and those with vertical layering (VL). Fig. 2 provides a conceptual picture of these specimens.

During this investigation, the static compaction method was utilized to achieve uniform compaction, homogeneity, and reproducibility among the specimens. The Marshall Compactor machine was used to produce necessary static compaction. The specimen was set up at 30 mm high and 50 mm wide. Static compaction prepares the specimen. HL and VL orientations change specimen layering. VL shows parallel soil layering, while HL shows perpendicular.

The dry density and water content of the compaction curve determine the soil specimen's preparation. After uniformly mixing the contents, the sample was compacted layer by layer in a 50 mm-diameter mold. Three-layer specimens were created. Each layer was compacted at 1 mm/min. After compaction, the specimen was extruded from the mold to provide a standard specimen for testing. VL samples required more dirt and compaction. To accommodate the ingredients, larger molds were employed. The 100-mm molds compacted seven layers. Extrusion followed compaction, like HL. The specimen dimension did not satisfy the norm, hence trimming was needed. Priono *et al.* (2016a) arranged rectangular and circular trim. Next test utilized trimmed specimen.

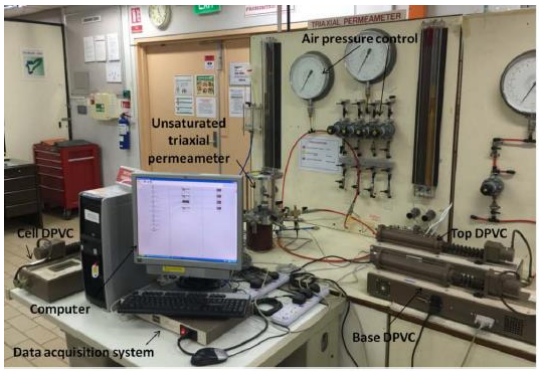

Fig. 3 Fully assembled unsaturated triaxial permeameter

5. Permeability and SWCC testing

A 50 mm in diameter and 30 mm in height soil sample was placed in a saturated triaxial permeameter for saturated permeability testing. Mold and vacuum gauge were used to cover the specimen with impervious membrane. Two sets of pedestals (top and bottom) capped the soil, with porous stone and filter paper in between. Finally, the triaxial permeameter was filled with distilled water and covered with plexiglass.

This test included saturation, consolidation, and saturated permeability. The digital pressure and volume controller (DPVC) incrementally applied cell and back pressure to saturate the soil. The next phase began when the pore pressure coefficient (B value) reached 0.95, indicating a fully saturated condition. Soil consolidation applied isotropic confining pressure. 25 kPa confining pressure usually consolidated the specimen without volume change. Saturated permeability testing concluded. For soil specimen upward flow, hydraulic gradient was addressed. Thus, top pedestal back pressure is lower than bottom pedestal base pressure. Inflow and outflow of DPVCs connected to the bottom and top pedestals recorded volume changes due to head pressure. Darcy's Law determined the saturated permeability coefficient from all data.

Following Priono *et al.* (2016a), SWCC tests were performed using axis-translation (Fredlund and Rahardjo, 1993). This approach converts negative pore-water pressure to pore-air pressure. This method maintained suction at 1 atm negative pressure without water cavitation. SWCC testing also followed saturated permeability test design. A porous stone was set atop the soil sample, while a ceramic disk was placed beneath it. DPVCs applied pressure and measured volume change during tests. SWCC test setup is presented in Fig. 3.

6. Test results

The values of the index soil properties are presented in Table 2. Due to the even distribution of sand and kaolin, specimens with a composition of 50S50K were classified as silty sand to sandy silt with low plasticity (SM-ML). In contrast, specimens with a composition of 30S70K were classified as silt with high plasticity (MH) because of the abundance of kaolin in the soil mixture.

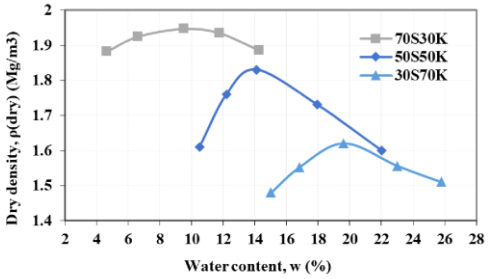

Fig. 4 Compaction curves of investigated soil mixtures (Specimen 1-6)

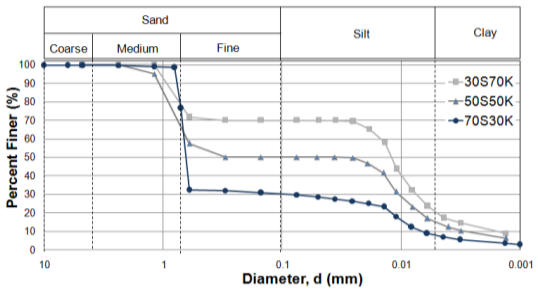

Fig. 5 GSD curve of the investigated soil specimens

Table 2 Index properties of the investigated soil mixtures

Index properties / Specimen #	1	2	3	4	5	6
Specific gravity, G_s	2.63	2.63	2.59	2.59	2.65	2.65
Liquid Limit, LL (%)	53	53	46.7	46.7	26.8	26.8
Plastic Limit, PL (%)	31	31	27.4	27.4	11.6	11.6
Plasticity Index, PI (%)	22	22	19.3	19.3	15.2	15.2
Dry Density, γ_d (Mg/m^3)	1.53	1.53	1.75	1.75	1.85	1.85
Water Content, w (%)	24.5	16	17.5	12.1	4.0	15.5
Sand (%)	30.0	30.0	50.0	50.0	70.0	70.0
Silt (%)	63.4	63.4	37.5	37.5	25.3	25.3
Clay (%)	6.6	6.6	12.5	12.5	4.7	4.7
Unified Soil Classification System (USCS)	MH	MH	SM-ML	SM-ML	SM	SM

Fig. 4 presents the compaction curves of the soil specimens under investigation, depicting the observed water content against the dry density obtained from the standard proctor compaction test. Specimens 5 and 6, corresponding to the 70S30K compaction curve, exhibit a maximum dry density of 1.947 Mg/m³ and an optimal water content of 9.5%. In addition, specimens 1 and 2 (30S70K), which underwent similar initial conditions as specimens 3 and 4 (50S50K), demonstrate a lower dry density.

Fig. 5 is a representation of the GSD curves of investigated specimens. Due to the presence of two humps or sub-curves in the GSD curve, it can be deduced that specimens contain gap-graded soil. In addition, silt-sized kaolin was found to predominate among the fine-grained particles, while medium-sized sand was found to predominate among the coarse-grained particles.

In the table that follows, the saturated permeability coefficients of specimens 1 through 6 are provided. Since water moved through the VL specimen at a far faster pace than it did through the HL specimen, the saturated permeability of the VL specimen was significantly higher than that of the HL specimen. The saturated permeability at

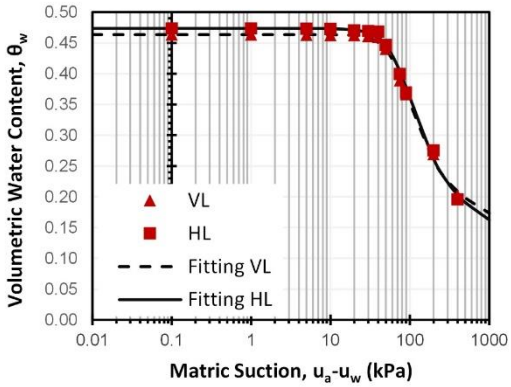

Fig. 6 Drying path SWCC of the Specimen 1 30S70K compacted at wet of optimum

Table 3 Saturated permeability coefficients and hydraulic anisotropy values of the soil samples

Specimen #	Hydraulic Anisotropy	$k_{sat, HL}$ (10^{-9} m/s)	$k_{sat, VL}$ (10^{-9} m/s)
1	4.26	0.5	2.2
2	2.16	9.3	20.1
3	5.83	1.9	11.2
4	3.20	16.7	53.4
5	9.06	9.6	89.2
6	5.39	54.5	294.0

30S70K is lower than that at 50S50K. The saturated permeability of each soil mixture's specimens compacted at the wet of optimal was lower when compared to specimens compacted at the dry of optimum. The disparity in permeability coefficients between HL and VL can be interpreted as evidence of the existence of hydraulic anisotropy. At every initial condition, the values of hydraulic anisotropy for 30S70K are lower than those for 50S50K.

Figs. 6 to 9 display the soil-water characteristic curves (SWCCs) of Specimens 1 to 4, respectively. For the unimodal SWCC shapes of Specimens 1 and 3, Eq. (1) provided the best fit, while Eq. (2) yielded the best fit for the bimodal SWCC shapes of Specimens 2 and 4. Each SWCC has a morphology consistent with previous research (Satyanaga *et al.* 2019, Priono *et al.* 2016b): a unimodal SWCC is produced by specimens compacted at wet optimum, whereas a bimodal SWCC is produced by specimens compressed at dry optimum. Throughout the

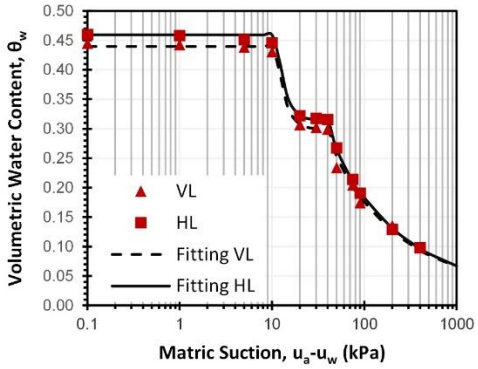

Fig. 7 Drying path SWCC of the Specimen 2 30S70K compacted at dry of optimum

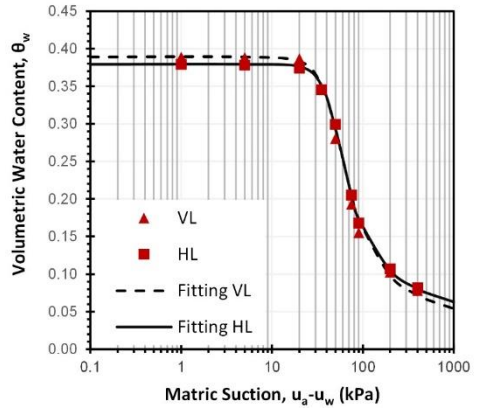

Fig. 8 Drying path SWCC of the Specimen 3 50S50K compacted at wet of optimum

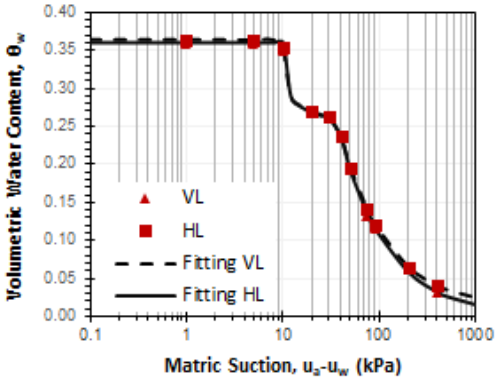

Fig. 9 Drying path SWCC of the Specimen 4 50S50K compacted at dry of optimum

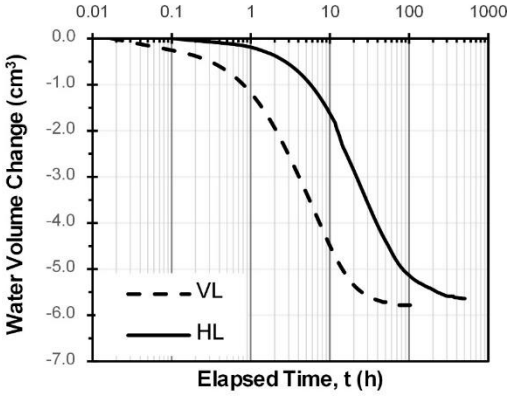

Fig. 10 Normalized rate of change in water volume versus time graph

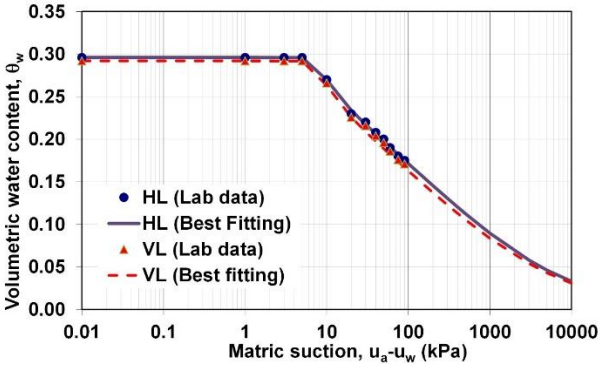

Fig. 11 SWCC of specimen 5

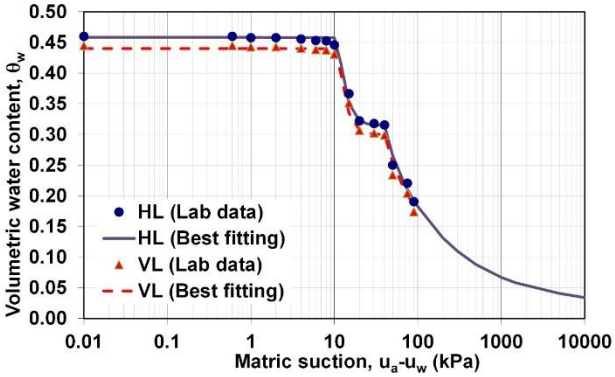

Fig. 12 SWCC of specimen 6

drying route SWCC, it was noted that the data points for HL and VL specimens were very comparable. For instance, in Specimen 1, the air-entry values for both the horizontal and vertical layers were recorded as 9 kPa. Similarly, in Specimen 2, these values were 43 kPa and 44 kPa for the horizontal and vertical layers, respectively.

It appeared that HL and VL specimens required different amounts of time to reach equilibrium or steady state (i.e., equalization time). Tests conducted with matric suction applications greater than the AEV value revealed this distinction. Fig. 10 depicts the normalized rate of change in water volume versus time. Similar to the SWCC, the curve is sigmoidal, and the final water volume change for HL and VL is roughly the same. When comparing VL and HL orientation specimens, the time required for equalization is less for the VL orientation. The water volume change was negligible in the matric suction application below AEV, and the equalization times of HL and VL specimens seemed comparable.

Figs. 11 and 12 show the SWCC analysis results for samples 5 and 6. Since Specimen 5's SWCC is sigmoidal, or has only one sub-curve, we classify it as soil with unimodal SWCC. Since there are two distinct sub-curves in the SWCC of Specimen 6, we label it bimodal SWCC soil.

7. Discussions

The dry density of the 30S70K specimen (95% γ_d is 1.53 Mg/m^3) at the corresponding starting compaction settings was lower than that of the 50S50K specimen (1.75 Mg/m^3), as shown by the compaction curve. The GSD curves for both samples are gap-graded, indicating two distinct distributions. Specimen 2, compacted at dry of optimum, appears to display bimodal SWCC similarly. Specimen 1, on the other hand, shows unimodal SWCC because it was compacted at the wet of optimum. These results are consistent with previous research showing that bimodality in the GSD curve can lead to either bimodal or unimodal SWCC (Li and Zhang 2009, Satyanaga *et al*. 2013). Under ideal drying conditions, the soil's pore size distribution (PSD) is not likely to change; therefore, the soil water content curve (SWCC) will maintain its characteristic bimodal distribution. On the other hand, when conditions are less than ideal, the PSD may shift, leading to SWCC, which has a unimodal form.

Based on the data shown in Table 3, it is clear that the coefficient of permeability is higher for the VL orientation than it is for the HL orientation when the sample is saturated. One possible explanation is that, in VL orientation, water flows parallel to the layered surface. There will be less resistance to water passage via the pores of the compacted surface. In addition, it was found that the 30S70K specimen's saturated permeability was less than that of the 50S50K specimen under both initial and operating circumstances. The high concentration of kaolin in the 30S70K blend creates more cohesiveness, restricting the passage of water.

The ratio of the two permeability coefficients ($k_{s,VL}$, $k_{s,HL}$) under saturated conditions is a measure of hydraulic anisotropy. Table 3 summarizes the data on the hydraulic anisotropy of investigated specimens. As a first point, hydraulic anisotropy is greater in soil samples compacted at the wet of optimal than those compacted at the dry of optimum, even though the two conditions are applied to the identical soil combination. It may be because soils at dry of optimum have a flocculated structure, while soils at wet of optimum have a scattered structure (Basak 1972). In contrast to the scattered structure, which might impede water flow in some directions, the flocculated structure allows water to move more freely throughout the soil. This structural difference in the soil may also explain why dry-of-optimum-compacted specimens are more permeable than wet-of-optimum-compacted ones.

Second, independent of starting conditions, the hydraulic anisotropy of the 30S70K specimen is smaller than that of the 50S50K specimen. The hydraulic anisotropy ratio of 30S70K in ideal dry conditions is 2.2, while that of 50S50K is 3.2. The ratio of hydraulic anisotropy is 4.3 for 30S70K and 5.8 for 50S50K under ideal wet conditions. The decreased dry density of the 30S70K specimen in comparison to the 50S50K specimen could be a contributing factor. It is consistent with research showing that density significantly impacts hydraulic anisotropy. Compared to less dense soils of the same volume, denser soils have fewer pores. Therefore, pore-water connectivity varies more across directions in soil with a higher particle density (i.e., there are more barriers to water flow).

Table 4. SWCC fitting parameters of 30S70K Specimens 1 and 2

Fitting Parameters	Specimen 1		Fitting Parameters	Specimen 2	
	HL	VL		HL	VL
θ_{s1}	0.460	0.445	θ_s	0.473	0.464
ψ_{a1}	9.000	9.000	a	71.384	67.246
ψ_{m1}	12.000	12.000	n	2.864	3.299
s_1	0.800	0.800	m	0.528	0.450
θ_{s2}	0.315	0.300	**R^2**	**0.995**	**0.996**
ψ_{a2}	43.000	40.000			
ψ_{m2}	98.000	98.000			
s_2	2.130	2.350			
ψ_r	1000.000	1000.000			
θ_r	0.050	0.049			
R^2	**0.998**	**0.994**			

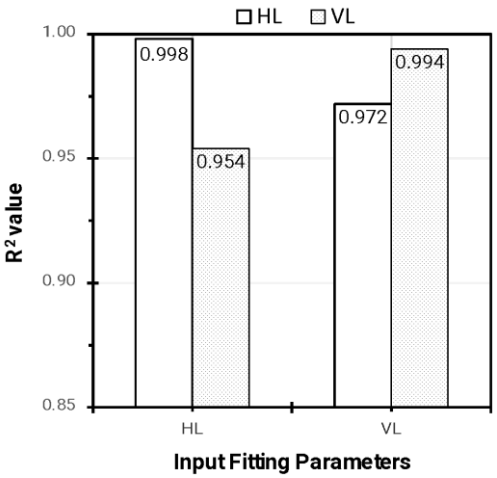

Fig. 13 Cross-input of Specimen 1 fitting parameters

Indirectly, the associated SWCC can represent properties of hydraulic anisotropy. Eq. (1) was used for unimodal shapes, while for bimodal shapes, Eq. (2) was used to find the best-fitting SWCC. Visually, SWCC looks to have the same form as the observed sites of unsaturated permeability. The reason for this is that the soil-water retention capacity (SWRC) is directly correlated with the permeability of the soil. As a result, permeability will vary between matric suction applications in the same manner as SWCC.

Table 4 presents the unimodal and bimodal fitting parameters for 30S70K Specimens 1 and 2. The best-fittingness to the SWCC measurements was evaluated using the coefficient of determination (R^2). The R^2 values for all samples are quite close to 1, which indicates distinguishable bi- and unimodal morphologies for samples compacted at dry and wet of optimum, respectively. The fitting parameters for HL and VL data points are comparable enough to be utilized interchangeably. Figs. 13 and 14 demonstrate the contrasting outcomes of this study. The

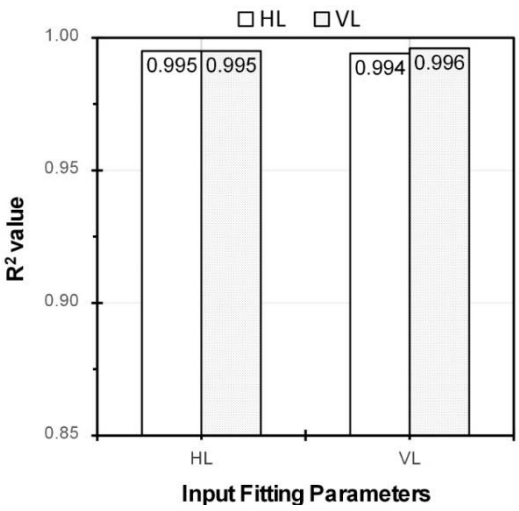

Fig. 14 Cross-input of Specimen 2 fitting parameters

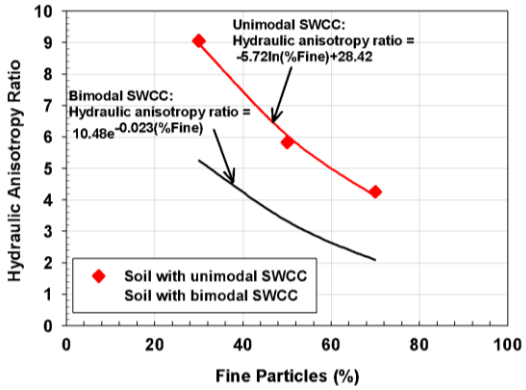

Fig. 15 Correlation between the hydraulic anisotropy ratio and the percentage of fine particles

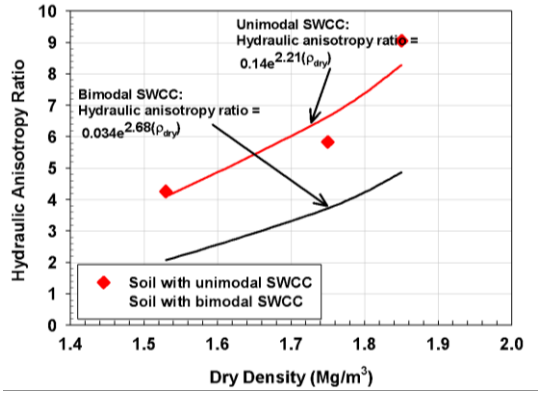

Fig. 16 Correlation between the hydraulic anisotropy ratio a nd the dry density

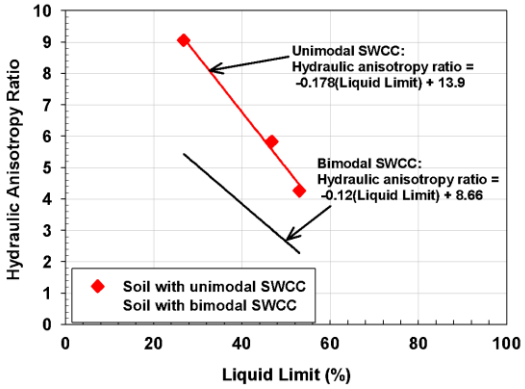

Fig. 17 Correlation between the hydraulic anisotropy ratio and the liquid limit

average R^2 value for 30S70K Specimen 1 is 0.980, according to the calculations. The calculated mean R^2 for 30S70K Specimen 2 is 0.995. Given a common starting point, the fairly high R2 values show that the same parameters of the best-fitting model can be used for both HL and VL specimens. Since there is no noticeable change in SWCC between HL and VL specimens, SWCC can be considered a scalar property. This finding supports the fact that continuous hydraulic anisotropy was seen along the drying path.

Three different compacted soil combinations had their soil characteristics and hydraulic anisotropy analyzed statistically. Figs. 15 and 16 depict that the impact of fine particles and dry density on hydraulic anisotropy, respectively.

Fig. 15 shows that the ratio of hydraulic anisotropy for unimodal and bimodal SWCC soils decreases nonlinearly with increasing fine contents in soil samples. Soil pores with a significant volume of tiny particles may be at fault, as they allow water to permeate more slowly. It was because the soil particles were arranged to allow for more micro- than macro-sized pores. It takes more time for water to move via micro-pores and less time through macro-pores. Because there were fewer macro-pores in the soil particle, the hydraulic anisotropy ratio was lower for samples containing a greater concentration of fine particles. However, the hydraulic anisotropy ratio and water penetration are both increased in soils with a higher percentage of coarse particles because of the increased number of macro-pores in such soils. Soil with unimodal SWCC has increased hydraulic anisotropy for varying percentages of fine particles, as seen in Fig. 15. Eqs. (4) and (5) show the hydraulic anisotropy ratio in terms of fine particle percentage for unimodal and bimodal SWCCs, respectively.

Unimodal SWCC:

$$Hydraulic\ anisotropy\ ratio = \quad (4)$$
$$= -5.7\ ln\ ln\ (Fine\ particles) + 28.4$$

Bimodal SWCC:

$$Hydraulic\ anisotropy\ ratio = \quad (5)$$
$$= 10.4e^{-0.02(Fine\ particles)}$$

According to Fredlund and Rahardjo (1993), the dispersed soil structure of Specimen 1 is to blame for this increased hydraulic anisotropy. Fig. 16 demonstrates the non-linear increase of hydraulic anisotropy ratios for soils with unimodal and bimodal soil-water characteristic curves (SWCC) as dry density increases. Eqs. (6) and (7) show the hydraulic anisotropy ratio in terms of dry density for unimodal and bimodal SWCCs, respectively.

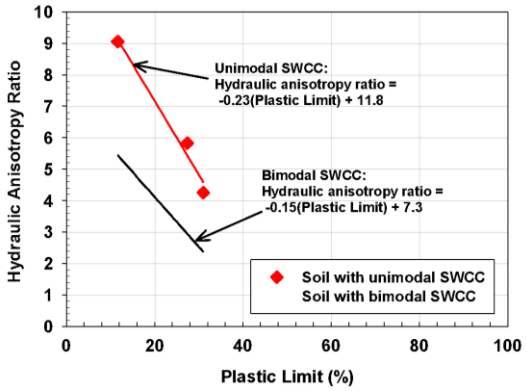

Fig. 18 Correlation between the hydraulic anisotropy ratio and the plastic limit

Unimodal SWCC:

$$Hydraulic\ anisotropy\ ratio = \\ = 0.14e^{2.2(Dry\ density)} \quad (6)$$

Bimodal SWCC:

$$Hydraulic\ anisotropy\ ratio = \\ = 0.031e^{2.7(Dry\ density)} \quad (7)$$

This trend can be attributed to the difference in soil structure between low-dry-density and high-dry-density specimens. Low-dry-density soil exhibits a less compacted structure compared to high-dry-density soil, resulting in reduced directional variation in pore-water connectivity. Consequently, low-dry-density soil exhibits lower levels of anisotropy compared to high-dry-density soil.

Figs. 17 and 18 exhibit a consistent trend between the plastic limit and the liquid limit as a function of the hydraulic anisotropy ratio. As the liquid limit and plastic limit of a soil specimen decline, the hydraulic anisotropy ratio grows linearly. Since the particle surface is wet and the pores are packed with water, water can easily permeate through the soil specimen with a high moisture content, explaining the phenomenon. Therefore, the ratio of hydraulic anisotropy is greater for the water with a larger liquid limit. The hydraulic anisotropy ratio in terms of liquid limit for the unimodal and bimodal SWCCs is shown in Eqs. (8) and (9), respectively. In contrast, the hydraulic anisotropy ratio in terms of plastic limit is shown in Eqs. (10) and (11), respectively.

Unimodal SWCC:

$$Hydraulic\ anisotropy\ ratio = \\ = -0.18(Liquid\ limit) + 13.9 \quad (8)$$

Bimodal SWCC:

$$Hydraulic\ anisotropy\ ratio = \\ = -0.12(Liquid\ limit) + 8.64 \quad (9)$$

Unimodal SWCC:

$$Hydraulic\ anisotropy\ ratio = \\ = -0.23(Plastic\ limit) + 11.8 \quad (10)$$

Bimodal SWCC:

$$Hydraulic\ anisotropy\ ratio = \\ = -0.16(Plastic\ limit) + 7.3 \quad (11)$$

8. Conclusions

The following can be stated as the summary of this study:

1. The hydraulic anisotropy of a soil specimen tested at dry of optimum conditions was lower than that of a soil specimen compacted at wet of optimum conditions. In other words, when comparing two soil specimens with the same dry density but different water contents, the specimen with higher water content displayed a higher hydraulic anisotropy than the specimen with lower water content.
2. The SWCC is considered a scalar property unaffected by the direction in which the layers are stacked. Consequently, a statistical model capable of estimating unsaturated permeability can be indirectly employed to determine hydraulic anisotropy.
3. It was discovered that dry density is a significant component in developing hydraulic anisotropy. The 30S70K specimen, which had a greater fines content but a lower dry density than the 50S50K specimen, had a lower hydraulic anisotropy ratio than the latter.
4. The hydraulic anisotropy of oil that contains a larger percentage of fines is lower when compared to the hydraulic anisotropy of soil that contains a lower percentage of particles.
5. Soils with higher liquid and plastic limits exhibit lower hydraulic anisotropy than soils with lower liquid and plastic limits. It can be attributed to higher liquid and plastic limits contributing to greater soil stability.

Acknowledgments

This research was supported by the Nazarbayev University Research Fund under Faculty Development Competitive Research Grants Program (FDCRGP) Grant No. 20122022FD4133. The authors are grateful for this support. Any opinions, findings, and conclusions or recommendations expressed in this material are those of the author(s) and do not necessarily reflect the views of the Nazarbayev University.

References

Al-Mahbashi, A.M., Elkady, T.Y. and Alrefeai, T.O. (2015), "Soil water characteristic curve and improvement in lime treated expansive soil", *Geomech. Eng.*, **8**(5), 687-696. https://doi.org/10.12989/gae.2015.8.5.687.

ASTM/D2487-11 (2011), "Standard practice for classification of soils for engineering purposes (Unified Soil Classification System)", Annual Book of ASTM Standards, ASTM International, West Conshohocken, PA. https://doi.org/10.1520/D2487-17.

ASTM/D422-63e2 (2007), "Standard test method for particle-size

analysis of soils", Annual Book of ASTM Standards, ASTM International, West Conshohocken, PA. https://doi.org/10.1520/D2487-17.

ASTM/D4318-10e1 (2010), "Standard test methods for liquid limit, plastic limit, and plasticity index of soils", Annual Book of ASTM Standards, ASTM International, West Conshohocken, PA. https://doi.org/10.1520/D4318-17E01.

ASTM/D698-12e1 (2012), "Standard test methods for laboratory compaction characteristics of soil using standard effort", Annual Book of ASTM Standards, ASTM International, West Conshohocken, PA. https://doi.org/10.1520/D2487-17.

ASTM/D7664-10 (2010), "Standard test methods for measurement of hydraulic conductivity of unsaturated soils", Annual Book of ASTM Standards, ASTM International, West Conshohocken, PA. https://doi.org/10.1520/D2487-17.

ASTM/D854-14 (2014), "Standard test methods for specific gravity of soil solids by water pycnometer", Annual Book of ASTM Standards, ASTM International, West Conshohocken, PA. https://doi.org/10.1520/D2487-17.

Assouline, S. and Or, D. (2006), "Anisotropy factor of saturated and unsaturated soils", *Water Resour. Res*., **42**, W12403. https://doi.org/10.1029/2006WR005001.

Basak, P. (1972), "Soil structure and its effects on hydraulic conductivity", *Soil Sci*., **114**(6), 417-422. https://doi.org/10.1097/00010694-197212000-00003.

Bear, J. and Cheng, A.H. D. (2010), "Modeling groundwater flow and contaminant transport", New York: Springer. https://doi.org/10.1007/978-1-4020-6682-5.

Chapuis, R.P., Gill, D.E. and Baass, K. (1989), "Laboratory permeability tests on sand: influence of the compaction method on anisotropy", *Can. Geotech. J*., **26**, 614-622. https://doi.org/10.1139/t91-022.

Deng, D., Wen, S., Lu, K. and Li, L. (2020), "Calculation model for the shear strength of unsaturated soil under nonlinear strength theory", *Geomech. Eng*., **21**(3), 247-258. https://doi.org/10.12989/gae.2020.21.3.247.

Deng, D., Lu, K. and Li, L. (2019), "LE analysis on unsaturated slope stability with introduction of nonlinearity of soil strength", *Geomech. Eng*., **19**(2), 179-191. https://doi.org/10.12989/gae.2019.19.2.179.

Fredlund, D.G. and Rahardjo, H. (1993), "Soil mechanics for unsaturated soils", New York: John Wiley and Sons Inc. https://doi.org/10.1002/9780470172759.

Fredlund, D.G. and Xing, A. (1994), "Equations for the soil–water characteristic curve", *Can. Geotech. J*., **31**, 521-532. https://doi.org/10.1139/t94-06.

Hamdany, A.H., Wijaya, M., Satyanaga, A., Rahardjo, H., Zhai, Q., Lim, A. and Kim, J. (2023), "Numerical simulation on the effect of infiltration and evapotranspiration on the residual slope", *Sustainability*, **15**(11), 8653. https://doi.org/10.3390/su15118653.

Kim, Y. and Jeong, S. (2017), "Modeling of shallow landslides in an unsaturated soil slope using a coupled model", *Geomech. Eng*., **13**(2), 353-370. https://doi.org/10.12989/gae.2017.13.2.353.

Krisnanto, S., Rahardjo, H. and Leong, E.C. (2020), "Numerical study on the effect of crack network representation on water content in cracked soil", *Geomech. Eng*., **21**(6), 537-549. https://doi.org/10.12989/gae.2020.21.6.537.

Lee, J.S., Guimaraes, M. and Santamarina, J.C. (2007), "Micaceous sands: microscale mechanisms and macroscale response", *J. Geotech. Geoenviron. Eng*., **133**(9), 1136-1143. https://doi.org/10.1061/(ASCE)1090-0241(2007)133:9(1136).

Leong, E.C. and Rahardjo, H. (1997), "Review of soil–water characteristic curve equations", *J. Geotech. Geoenviron. Eng*., **123**(12), 1106-1117. https://doi.org/10.1061/(ASCE)1090-0241(1997)123:12(1106).

Li, X. and Zhang, L.M. (2009), "Characterization of dual-structure pore-size distribution of soil", *Can. Geotech. J*., **46**(2), 129-141. https://doi.org/10.1139/T08-110.

Mualem, Y. (1984), "Anisotropy of unsaturated soils", *Soil Sci. Soc. Am. J*., **48**, 505-509. https://doi.org/10.2136/sssaj1984.03615995004800030007x.

Mualem, Y. (1986), "Hydraulic conductivity of unsaturated soils: prediction and formulas. In Methods of soil analysis. Part 1: Physical and mineralogical methods", 2nd Ed., 799-823, Agronomy, American Society of Agronomy, Inc., and Soil Science Society of America, Madison, Wisc. https://doi.org/10.2136/sssabookser5.1.2ed.c31.

Priono, Rahardjo, H., Chatterjea, K., Leong, E.C. and Wang, J.Y. (2016a), "Effect of hydraulic anisotropy on soil-water characteristic curve", *Soils Found*., **56**(2), 228-239. https://doi.org/10.1016/j.sandf.2016.02.006.

Priono, Rahardjo, H., Leong, E.C. and Chatterjea, K. (2016b), "Effects of mica content on hydraulic anisotropy of unsaturated soil", *Proceedings of the 12th International Symposium on Landslides*, Naples, Italy. https://doi.org/10.1201/9781315375007-197.

Qi, S., Vanapalli, S.K., Yang, X.G., Zhou, J.W. and Lu, G.D. (2019), "Stability analysis of an unsaturated expansive soil slope subjected to rainfall infiltration", *Geomech. Eng*., **19**(1). https://doi.org/10.12989/gae.2019.19.1.011.

Rahardjo, H., Meilani, I., Rezaur, R.B. and Leong, E.C. (2009), "Shear strength characteristics of a compacted soil under infiltration conditions", *Geomech. Eng*., **1**(1), 35-52. https://doi.org/10.12989/gae.2009.1.1.035.

Roth, K. and Hammel, K. (1996), "Transport of conservative chemical through an unsaturated two-dimensional Miller-similar medium with steady-state flow", *Water Resour. Res*., **32**(6), 1653-1663. https://doi.org/10.1029/96WR00756.

Satyanaga, A. and Rahardjo, H. (2022), "Role of unsaturated soil properties in the development of slope susceptibility map", *Proceedings of the Institution of Civil Engineers-Geotechnical Engineering*, **175**(3), 276-288. https://doi.org/10.1680/jgeen.20.00085.

Satyanaga, A., Bairakhmetov, N., Kim, J.R. and Moon, S.W. (2022), "Role of bimodal water retention curve on the unsaturated shear strength", *Appl. Sci*., **12**(3), 1266. https://doi.org/10.3390/app12031266.

Satyanaga, A., Rahardjo, H., Koh, Z.H. and Mohamed, H. (2019a), "Measurement of a soil-water characteristic curve and unsaturated permeability using the evaporation method and the chilled-mirror method", *J. Zhejiang Univ.-Sci. A*, **20**(5), 368-374. https://doi.org/10.1631/jzus.A1800593.

Satyanaga, A., Rahardjo, H. and Hua, C.J. (2019b), "Numerical simulation of capillary barrier system under rainfall infiltration in Singapore", *ISSMGE Int. J. Geoengineering Case Histories*, **5**(1), 43-54. https://doi.org/10.4417/IJGCH-05-01-04.

Sharipov, A., Satyanaga, A., Abishev, R., Moon, S., Taib, A.M. and Kim, J. (2023). "Influence of slope geometry on stability of clayey soil slopes", *Geotech. Geol. Eng*., https://doi.org/10.1007/s10706-023-02438-0.

Ursino, N., Roth, K., Gimmi, T. and Fluhner, H. (2000), "Upscaling of anisotropy in unsaturated Miller-similar porous media", *Water Resour. Res*., **36**(2), 421-430. https://doi.org/10.1029/1999WR900320.

Zhai, Q., Zhu, Y., Rahardjo, H., Satyanaga, A., Dai, G., Gong, W., Zhao, X. and Ou, Y. (2023), "Prediction of the soil–water characteristic curves for the fine-grained soils with different initial void ratios", *Acta Geotechnica*, https://doi.org/10.1007/s11440-023-01833-4.

Zhai, Q., Rahardjo, H., Satyanaga, A. and Dai, G. (2020a), "Estimation of tensile strength of sandy soil from soil–water characteristic curve", *Acta Geotechnica*, **15**, 3371-3381.

https://doi.org/10.1007/s11440-020-01013-8.
Zhai, Q., Rahardjo, H., Satyanaga, A., Dai, G.L. and Du, Y.J. (2020b), "Effect of the uncertainty in soil-water characteristic curve on the estimated shear strength of unsaturated soil", *J. Zhejiang Univ.: Sci. A*., https://doi.org/10.1631/jzus.A1900589.
Zhai, Q., Rahardjo, H., Satyanaga, A., Dai, G. and Du, Y. (2020c), "Estimation of the wetting scanning curves for sandy soils", Eng. Geol., **272**, 105635. https://doi.org/10.1016/j.enggeo.2020.105635.

IC